nature neuroscience

Locus-specific epigenetic remodeling controls addiction- and depression-related behaviors

Elizabeth A Heller[1], Hannah M Cates[1], Catherine J Peña[1], Haosheng Sun[1], Ningyi Shao[1], Jian Feng[1], Sam A Golden[1], James P Herman[2], Jessica J Walsh[1,3], Michelle Mazei-Robison[1,9], Deveroux Ferguson[1,8], Scott Knight[4], Mark A Gerber[4], Christian Nievera[4], Ming-Hu Han[3], Scott J Russo[1], Carol S Tamminga[5], Rachael L Neve[6], Li Shen[1], H Steve Zhang[7], Feng Zhang[8] & Eric J Nestler[1]

Chronic exposure to drugs of abuse or stress regulates transcription factors, chromatin-modifying enzymes and histone post-translational modifications in discrete brain regions. Given the promiscuity of the enzymes involved, it has not yet been possible to obtain direct causal evidence to implicate the regulation of transcription and consequent behavioral plasticity by chromatin remodeling that occurs at a single gene. We investigated the mechanism linking chromatin dynamics to neurobiological phenomena by applying engineered transcription factors to selectively modify chromatin at a specific mouse gene *in vivo*. We found that histone methylation or acetylation at the *Fosb* locus in nucleus accumbens, a brain reward region, was sufficient to control drug- and stress-evoked transcriptional and behavioral responses via interactions with the endogenous transcriptional machinery. This approach allowed us to relate the epigenetic landscape at a given gene directly to regulation of its expression and to its subsequent effects on reward behavior.

Drug addiction and depression are associated with altered expression or activity of particular transcription factors and histone-modifying enzymes in both rodent models and human patients; experimental manipulation of such molecules in discrete brain regions alters the cellular and behavioral responses to drug or stress exposures in animals[1–4]. Studies of the mechanisms underlying altered gene expression in response to drugs or stress have involved analyses of transcription factor binding and enrichment of modified histones throughout the genome[5,6]. Notably, despite global enrichment in histone acetylation and depletion in histone methylation in a given brain region, many genes show alterations opposite to these, posing a key question as to the mechanism and relevance of gene-specific chromatin remodeling in the context of drug- and stress-evoked epigenetic changes. Although work to date has laid the foundation for investigating the role of such histone modifications in the regulation of drug or stress responses, previous approaches have lacked the specificity needed to demonstrate the causal mechanisms by which a given chromatin modification at a specific gene is necessary and sufficient to regulate drug- or stress-evoked transcriptional and behavioral plasticity.

To overcome this limitation, we focused on the transcription factor ΔFosB acting in the nucleus accumbens (NAc), a key brain reward region, during drug and stress action[7,8]. ΔFosB is induced in the NAc by chronic cocaine exposure in rodents and in human cocaine addicts[4,9], but its expression is reduced by certain forms of chronic stress in rodents and in depressed humans[10,11]. The histone methyltransferase G9a (EHMT2), which catalyzes dimethylation of histone H3 lysine 9 (H3K9me2), a repressive histone modification[12], appears to be crucial for mediating this regulation: H3K9me2 enrichment at *Fosb* is suppressed in the NAc by repeated cocaine[12], and we found increased levels of H3K9me2 at *FOSB* in the NAc of depressed humans. Moreover, we previously found that local overexpression or knockdown of G9a in NAc potently controls drug and stress responses in rodents[11,12]. Nevertheless, this quality of proof is inherently limited because drugs and stress, as well as G9a manipulations, affect H3K9me2 enrichment at hundreds of loci in this brain region[1,12,13]. These previous studies underscore the fact that all of the current evidence for the epigenetic basis of reward pathology has relied on correlating the effects of global manipulations of histone post-translational modifications (HPTMs) with affected behavior and physiology, resulting in a limited analysis of the transcriptional mechanisms linking epigenetic modifications at a single gene to the transcriptional activity of that gene and subsequent reward behavior.

We sought to achieve a stronger level of proof using engineered transcription factors, zinc-finger proteins (ZFPs)[14] or transcription activator-like effectors (TALEs)[15] that can be designed *in silico* to recognize and bind to a specific 18–20-bp locus in the genome. Fusion of the DNA-binding domain to a given catalytic domain allows gene-targeted transcriptional regulation at the site of interest. ZFPs and TALEs have been applied *in vitro* and have been shown to efficiently activate or repress gene expression when fused to any of several functional domains.

[1]Fishberg Department of Neuroscience and Friedman Brain Institute, Icahn School of Medicine at Mount Sinai, New York, New York, USA. [2]National Eye Institute, National Institutes of Health, Bethesda, Maryland, USA. [3]Department of Pharmacology and System Therapeutics, Icahn School of Medicine at Mount Sinai, New York, New York, USA. [4]Sigma Aldrich, Saint Louis, Missouri, USA. [5]Department of Psychiatry, University of Texas Southwestern Medical Center, Dallas, Texas, USA. [6]Department of Brain and Cognitive Sciences, Massachusetts Institute of Technology, Cambridge, Massachusetts, USA. [7]Sangamo Biosciences Inc., Richmond, California. [8]McGovern Institute for Brain Research, Massachusetts Institute of Technology, Cambridge, Massachusetts, USA. [8]Present address: Department of Basic Medical Sciences, University of Arizona College of Medicine, Phoenix, Arizona, USA (D.F.), Department of Physiology, Michigan State University, East Lansing, Michigan, USA (F.Z.). Correspondence should be addressed to E.J.N. (eric.nestler@mssm.edu).

Received 2 October; accepted 16 October; published online 27 October 2014; doi:10.1038/nn.3871

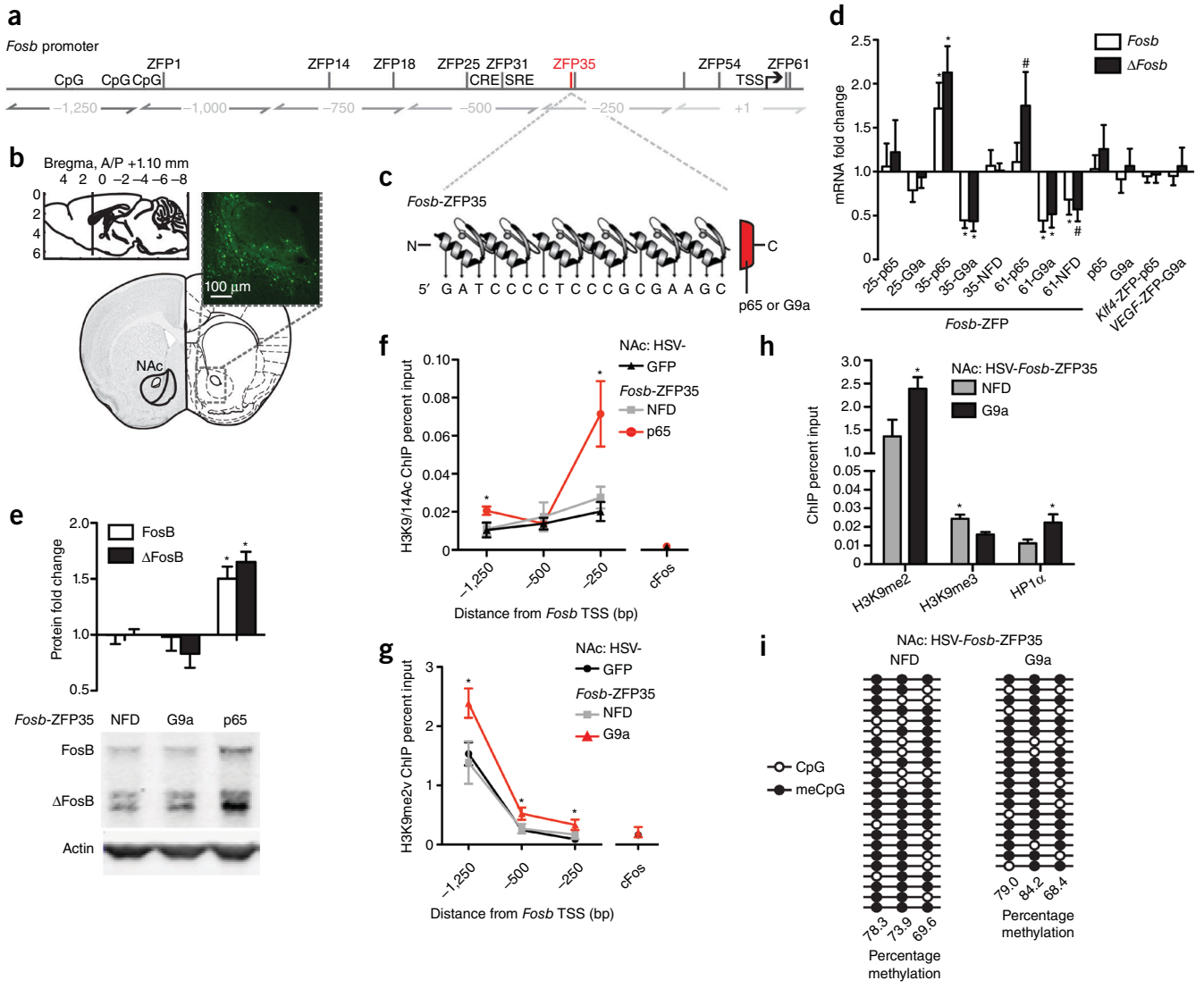

Figure 1 Engineered transcription factors targeting the *Fosb* promoter bidirectionally regulate gene expression in NAc neurons via epigenetic manipulation. (**a**) Locations of *Fosb*-ZFP binding relative to the *Fosb* TSS. The location of functional SRF and CREB binding sites are shown. CpG, methylation sites analyzed in **i**. (**b**) HSV injection into the mouse NAc[43] drove robust transgene expression in neurons. (**c**) The six-finger ZFP35 recognized the *Fosb* promoter ~250 bp upstream of the *Fosb* TSS. (**d**) At 72 h post-injection, *Fosb*/Δ*Fosb* mRNA expression in the NAc was significantly induced by HSV-*Fosb*-ZFP35-p65 compared with control virus (*Fosb*, $t_7 = 2.37$, $^*P = 0.049$; Δ*Fosb*, $t_7 = 3.83$, $^*P = 0.007$; $n = 4, 5$ mice per group), with a trend for Δ*Fosb* induction by *Fosb*-ZFP61-p65 ($t_7 = 2.03$, $^{\#}P = 0.076$; $n = 4, 5$). Compared with controls, *Fosb*/Δ*Fosb* mRNA in the NAc were significantly repressed by HSV-*Fosb*-ZFP35-G9a (*Fosb*, $t_6 = 4.84$, $^*P = 0.003$; Δ*Fosb*, $t_6 = 3.40$, $^*P = 0.015$; $n = 5, 3$), HSV-*Fosb*-ZFP61-NFD (*Fosb*, $t_7 = 2.39$, $^*P = 0.048$; $n = 4$), and *Fosb*-ZFP61-G9a (*Fosb*, $t_8 = 2.98$, $^*P = 0.017$; Δ*Fosb*, $t_8 = 2.37$, $^*P = 0.047$; $n = 5, 5$), with a trend for repression of ΔFosB by Fosb-ZFP61-NFD (Δ*Fosb*, $t_7 = 2.18$, $^{\#}P = 0.066$, $n = 5$). HSV-G9a, HSV-p65, HSV-*Klf4*-ZFP-p65, HSV-*VEGF*-ZFP-G9a and HSV-*Fosb*-ZFP35-NFD had no effect on *Fosb*/Δ*Fosb* mRNA expression (Student's unpaired *t* test, $P > 0.05$ for all other comparisons; **Supplementary Table 3**). (**e**) Compared with HSV-*Fosb*-ZFP35-NFD ($n = 9$ ChIP samples), NAc injection of HSV-*Fosb*-ZFP35-p65 resulted in increased FosB/ΔFosB protein levels (FosB, $t_{13} = 3.73$, $^*P = 0.003$; ΔFosB: $t_{13} = 6.65$, $^*P = 0.000$; $n = 6$), whereas HSV-*Fosb*-ZFP35-G9a had no effect at 72 h post-injection (FosB, $t_{14} = 0.137$, $P = 0.8929$; ΔFosB, $t_{14} = 1.25$, $P = 0.230$; $n = 8$). Representative western blots are shown. Full-length western blots are shown in **Supplementary Figure 5**. (**f**) NAc injection of HSV-*Fosb*-ZFP35-p65 caused enrichment of the activating mark H3K9/14ac at the *Fosb* promoter at –1,250 ($t_8 = 2.65$, $^*P = 0.029$, $n = 5, 5$ ChIP samples) and –250 bp ($t_8 = 2.9$, $^*P = 0.021$, $n = 5, 5$) relative to the TSS compared with control HSV, with no change in tissue treated with HSV-*Fosb*-ZFP35-NFD ($t_{10} = 0.00$, $P = 1.00$; $n = 6, 6$) or at the *Fos* promoter ($t_7 = 0.217$, $P = 0.834$; $n = 5, 4$). IgG control IP was undetectable in >80% of the sample wells by qRT-PCR. (**g**) NAc injection of HSV-*Fosb*-ZFP35-G9a caused enrichment of the repressive mark H3K9me2 at the *Fosb* promoter at –1,250 ($t_{26} = 2.7$, $^*P = 0.011$, $n = 14$, 14 ChIP samples), –500 ($t_{14} = 2.3$, $^*P = 0.041$, $n = 7, 9$) and –250 bp ($t_{13} = 2.9$, $^*P = 0.031$, $n = 7, 8$) relative to the TSS compared with control HSV, with no change in tissue treated with HSV-*Fosb*-ZFP35-NFD (–1,250, $t_{19} = 0.45$, $P = 0.658$, $n = 14, 7$; –500, $t_8 = 0.03$, $P = 0.977$, $n = 7, 3$; –250, $t_9 = 1.51$, $P = 0.167$, $n = 8, 3$) or at the *Fos* promoter ($t_{16} = 0.42$, $P = 0.680$ $n = 7, 11$). IgG control immunoprecipitation was undetectable in >80% of the sample wells by qPCR. (**h**) NAc injection of HSV-*Fosb*-ZFP35-G9a caused enrichment of H3K9me2 ($t_{19} = 2.4$, $^*P = 0.0238$, $n = 5, 5$) depletion of the repressive mark H3K9me3 ($t_8 = 3.3$, $^*P = 0.011$, $n = 5, 5$ ChIP samples) and enrichment of HP1α ($t_7 = 2.5$, $^*P = 0.039$, $n = 4, 4$) at the *Fosb* promoter –1,250 bp upstream from the TSS compared with control HSV-*Fosb*-ZFP35-NFD. (**i**) Bisulfite sequencing analysis performed on three CpG sites located –1,141, –1,101 and –1,036 bp upstream of the *Fosb* TSS, in a region that corresponds to the observed H3K9me2 and HP1α enrichment (**a**). There was no difference in the percentage of methylated CpGs in NAc infected with HSV-*Fosb*-ZFP35-G9a ($n = 19$ clones) compared with HSV-*Fosb*-ZFP35-NFD ($n = 23$). Each row represents analysis performed on one clone. Data are presented as mean ±s.e.m.

More recently, ZFPs and TALEs have been used *in vitro* to promote epigenetic remodeling when fused to chromatin-modifying enzymes[14,16,17]. Although very few studies to date have used this approach *in vivo*, one study showed reversal of a Parkinsonian phenotype in a mouse model by overexpression of a ZFP-transcriptional activator directed against the promoter of glial cell line–derived neurotrophic factor (*Gdnf*), which conferred protection from a striatal chemical lesion[18]. We took advantage of this approach to investigate the causal role of cocaine- and stress-evoked epigenetic regulation of the *Fosb* locus in the NAc *in vivo*.

RESULTS

Generation of ZFPs that target the *Fosb* gene *in vivo*

To direct locus-specific epigenetic changes to a specific gene, we screened a suite of cys2-his2 six-finger ZFPs[19] for regulation of *Fosb* transcription, designed *in silico* to span the murine *Fosb* promoter at various 18–20-bp motifs within −1,000 to +200 bp relative to the transcription start site (TSS) (**Fig. 1**). As an initial proof of principle, each ZFP was fused to the p65 domain of the mammalian transcription factor NFκB, which activates transcription by promoting histone acetylation via recruitment of p300/CBP (CREB-binding protein)[20]. Histone acetylation has been shown to modulate drug- and stress-evoked behavior[21–23] and gene expression[1,24], in part by regulating drug-associated memory formation[25,26]. A subset of the *Fosb*-ZFP-p65 constructs were transfected into Neuro2a (N2a) cells and their relative efficacy was determined by quantitative reverse transcription PCR (qRT-PCR) analysis of *Fosb/ΔFosb* mRNA expression (**Supplementary Fig. 1**). ZFP25, ZFP35 and ZFP61 were selected as potent activators of *Fosb* transcription and subjected to further analysis. To study regulation of the *Fosb* gene *in vivo*, we injected mouse NAc (**Fig. 1b** and **Supplementary Fig. 2a**) with herpes simplex virus (HSV) vectors expressing various *Fosb*-ZFP-p65 or *Fosb*-ZFP-NFD (no functional domain) constructs and quantified *Fosb/ΔFosb* mRNA using qRT-PCR.

We found that HSV-*Fosb*-ZFP35 and HSV-*Fosb*-ZFP65-p65 constructs activated transcription of *Fosb/ΔFosb* in the NAc relative to HSV-GFP or HSV-NFDs (**Fig. 1d**). To address the mechanism of the repressive histone mark H3K9me2 in the regulation of *Fosb* expression, we generated *Fosb*-ZFP-G9a constructs, in which each of three distinct ZFPs was fused to the minimal catalytic domain of G9a[14,27]. HSV delivery of *Fosb*-ZFP35-G9a or *Fosb*-ZFP61-G9a to the NAc efficiently repressed *Fosb/ΔFosb* mRNA expression (**Fig. 1d**). The changes in the amount of *Fosb*/ΔFosb mRNA that we observed in the NAc were physiologically relevant and were similar in magnitude to drug- and stress-induced changes observed previously[1,24]. In addition to regulation of basal mRNA expression, we found by immunoblotting that FosB/ΔFosB protein was elevated in NAc expressing HSV-*Fosb*-ZFP35-p65 (**Fig. 1e**), whereas there was no effect in NAc infected with HSV-*Fosb*-ZFP35-G9a relative to the HSV-*Fosb*-ZFP35-NFD at 72 h post infection. To more carefully examine *Fosb* repression by HSV-*Fosb*-ZFP35-G9a, we performed immunohistochemistry and found that the percentage of FosB/ΔFosB-immunopositive cells decreased markedly as a percentage of HSV-infected (GFP^+) cells in NAc infected with HSV-*Fosb*-ZFP35-G9a compared with a control vector (**Supplementary Fig. 2b**). These findings confirm that the ZFPs were exerting their function in the HSV-infected neurons that expressed FosB/ΔFosB.

The ability to site-specifically regulate chromatin architecture enables direct examination of the function of HPTMs in regulating gene transcription in the brain. We used semiquantitative chromatin immunoprecipitation (qChIP; **Supplementary Table 1**) and found enrichment of the activating histone modification, H3K9/K14 acetylation, at the *Fosb* promoter (**Fig. 1f**) in NAc infected with HSV-*Fosb*-ZFP35-p65, an effect that was not observed in NAc infected with HSV-*Fosb*-ZFP35-G9a (**Fig. 2a**). Conversely, NAc infection with HSV-*Fosb*-ZFP35-G9a led to the enrichment of the repressive histone modification H3K9me2 at the *Fosb* promoter (**Fig. 1g**). Notably, H3K9me2 was not enriched at the promoter of the related immediate early gene *Fos* (**Fig. 1f**,**g**), nor was H3K9me2 enriched globally in total NAc extracts (H3K9me2: $t_{1,15} = 1.35$, $P = 0.20$, $n = 8$ NFD, $n = 9$ G9a). Taken together, these results demonstrate that viral expression of engineered ZFPs efficiently enrich their respective HPTMs at the *Fosb* promoter and bi-directionally control *Fosb* gene expression *in vivo*.

The analysis of control constructs was critical to our investigation, as both a ZFP with NFD[28] or the functional domain alone[29] may have nonspecific effects on transcription. We found that neither the p65 nor G9a domains alone regulated expression of *Fosb* when virally expressed in the NAc (**Fig. 1d**). Furthermore, ZFPs targeted to unrelated genes, *Klf4*-ZFP-p65 and *Vegf*-ZFP-G9a, did not affect *Fosb*/Δ*Fosb* expression in the NAc (**Fig. 1d**). Finally, NAc expression of HSV-*Fosb*-ZFP35-NFD had no effect on *Fosb*/Δ*Fosb* mRNA levels (**Fig. 1d**) or on enrichment of HPTMs at the *Fosb* promoter (**Fig. 1f**,**g**). We did find that *Fosb*-ZFP61-NFD repressed *Fosb* expression (**Fig. 1d**), perhaps because its binding site is just downstream of the TSS (**Fig. 1a**), and we therefore excluded this ZFP from further study.

To determine the specificity of *Fosb* gene regulation by *Fosb*-ZFP35, we examined the mouse genome for 19-bp motifs that differed from the ZFP35-binding motif by one, two or three nucleotides and were located in 3 kb of a TSS (no site shared the identical 19-bp sequence; **Supplementary Table 2**) and we found 28 off-target genes. Using qRT-PCR, we found that the expression of these 28 off-target genes was unaffected by NAc expression of HSV-*Fosb*-ZFP35-p65, HSV-*Fosb*-ZFP35-G9a or HSV-*Fosb*-ZFP35-NFD (22 genes) or was undetectable (6 genes) (**Fig. 2b**). Finally, we selected those loci located within 1,000 bp upstream of their respective TSSs and found that HSV-*Fosb*-ZFP35-G9a in NAc did not alter H3K9me2 binding at any of these six off-target sites (**Fig. 2c**). This detailed analysis of specificity goes further than previous studies to assess the off-target regulation by ZFPs *in vivo*. Nonetheless, we cannot rule out the possibility of undetected off-target regulation of additional genes that may contribute to the transcriptional and behavioral changes induced by *Fosb*-ZFP35-G9a or *Fosb*-ZFP35-p65. On the basis of this detailed characterization, we focused on *Fosb*-ZFP35.

Mechanisms of action of *Fosb*-ZFP-G9a in NAc

To investigate the potential mechanism by which enrichment of H3K9me2 in *Fosb* promoter regulates expression of *Fosb*/Δ*Fosb*, we examined additional histone modifications and histone-binding proteins that may contribute to gene repression. We found that expression of HSV-*Fosb*-ZFP-G9a in NAc did not alter enrichment of tri-methylated histone H3 lysine 27 (H3K27me3) or histone H3 lysine 4 (H3K4me3), which are repressive and activating marks, respectively, at the *Fosb* gene (**Fig. 2**). We next examined two marks that have been strongly implicated in repression, acting in concert with H3K9me2, tri-methylated histone H3 lysine 9 (H3K9me3) and heterochromatin protein 1α (HP1α)[30,31]. We found that HSV-*Fosb*-ZFP-G9a in NAc decreased the levels of H3K9me3, but induced a ~2-fold enrichment of HP1α, at the *Fosb* promoter compared with HSV-*Fosb*-ZFP-NFD (**Fig. 1h**). However, the level of H3K9me3 and HP1α binding to *Fosb* was nearly an order of magnitude below that of H3K9me2, raising the possibility that other factors are primarily involved in mediating *Fosb* repression associated with increased H3K9me2 at euchromatic regions in adult brain. Notably, both H3K9me3 depletion and HP1α enrichment were detected only at a site ~1,200 bp upstream from the *Fosb* TSS, which we found to be the major site of enrichment of H3K9me2 in response to HSV-*Fosb*-ZFP35-G9a (**Fig. 1g**) and under physiological conditions in both mouse[12,13] and human NAc (**Fig. 3g**). This site is ~1,000 bp upstream of the ZFP35 binding site (**Fig. 1a**), suggesting that the binding of G9a to a proximal

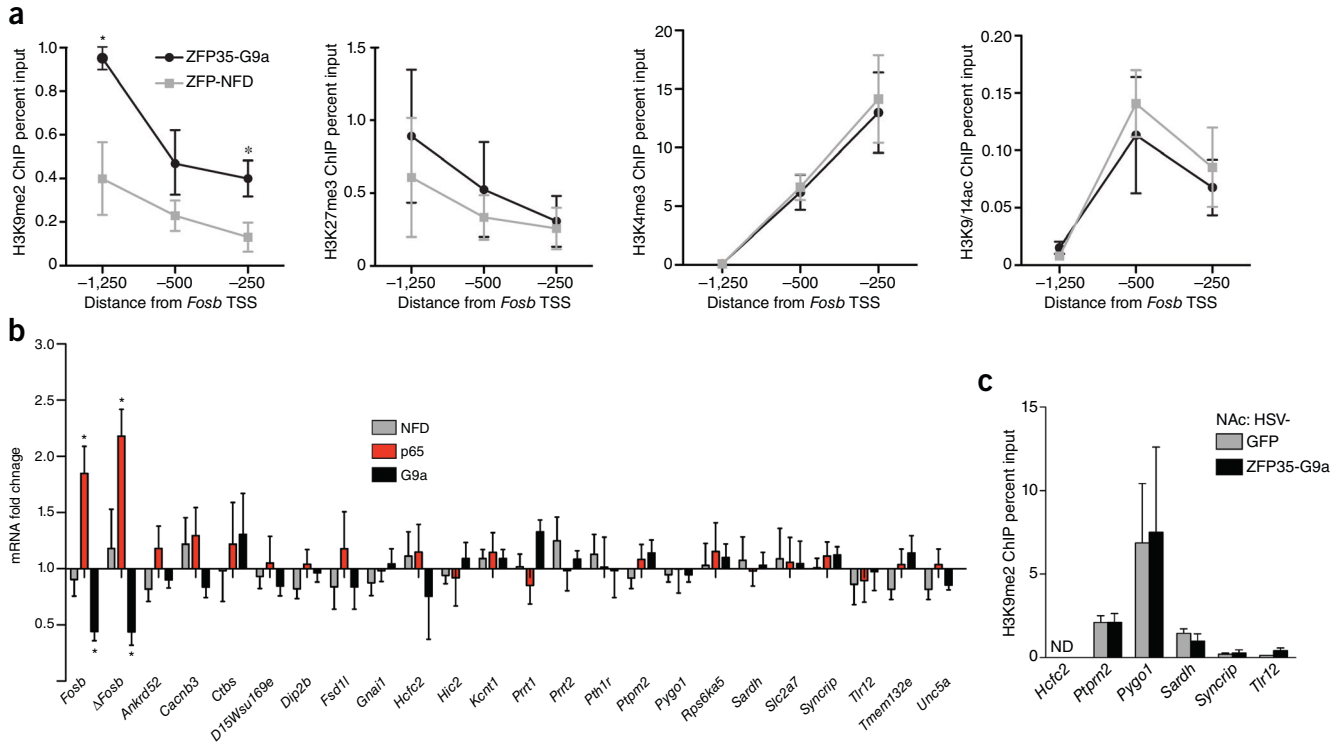

Figure 2 HSV-*Fosb*-ZFP35-p65 and -G9a in the NAc specifically regulate FosB/ΔFosB expression. (**a**) Induction of H3K9me2 at the *Fosb* promoter by HSV-*Fosb*-ZFP-G9a in NAc occurs relative to the TSS at –1,250 bp ($t_5 = 2.75$, $^*P = 0.040$, $n = 3$, 4 ChiP samples) and –250 bp ($t_5 = 2.69$, $^*P = 0.043$, $n = 3$, 4) without changes in the activating marks H3K9/14ac (–1,250, $t_5 = 1.49$, $P = 0.197$; –500, $t_5 = 0.50$, $P = 0.636$; –250, $t_5 = 0.39$, $P = 0.715$; $n = 3$, 4) or H3K4me3 (–1,250, $t_5 = 0.37$, $P = 0.728$; –500, $t_5 = 0.24$, $P = 0.820$; –250, $t_5 = 0.22$, $P = 0.835$; $n = 3$, 4) or the repressive mark H3K27me3 (–1,250, $t_5 = 0.46$, $P = 0.666$; –500, $t_5 = 0.59$, $P = 0.583$; –250, $t_5 = 0.23$, $P = 0.831$; $n = 3$, 4) as compared with the control (HSV-*Fosb*-ZFP-NFD). (**b**) cDNA was generated from NAc injected with HSV-*Fosb*-ZFP35-p65, HSV-*Fosb*-ZFP35-G9a or HSV-*Fosb*-ZFP35-NFD. qRT-PCR was used to measure expression of potential off-target genes (**Supplementary Table 2**) in samples that showed regulation of FosB/ΔFosB by HSV-*Fosb*-ZFP35-p65 (FosB, $t_7 = 4.73$, $^*P = 0.002$; ΔFosB, $t_7 = 4.83$, $^*P = 0.002$; $n = 4$, 5 mice) and HSV-*Fosb*-ZFP35-G9a (FosB, $t_8 = 2.40$, $^*P = 0.043$; ΔFosB, $t_8 = 2.88$, $^*P = 0.021$; $n = 5$, 5), but not HSV-*Fosb*-ZFP35-G9a (FosB: $t_8 = 0.38$, $P = 0.715$; ΔFosB: $t_8 = 0.52$, $P = 0.619$; $n = 5$, 5). Data were normalized to HSV-GFP (Student's unpaired *t* test, $P > 0.05$ for all other comparisons; **Supplementary Table 3**). (**c**) HSV-*Fosb*-ZFP35-G9a in the NAc did not cause H3K9me2 enrichment at off-target loci as measured by qChIP using primers that flank the off-target binding site (*Ptprn2*, $t_4 = 0.03$, $P = 0.97$; *Pygo1*, $t_5 = 0.10$, $P = 0.922$; *Sardh*, $t_4 = 0.93$, $P = 0.407$; *Syncrip*, $t_4 = 0.34$, $P = 0.775$; *Tlr12*, $t_4 = 1.80$, $P = 0.152$; $n = 3$, 3 ChiP samples). Data are presented as mean ±s.e.m.

site on the *Fosb* promoter induces a spreading repressive mechanism that affects a relatively large span of the *Fosb* gene. Based on these findings, we further investigated an additional epigenetic signature, DNA methylation. Although we observed methylation of the three predicted CpG sites in this ~1,200-bp region of *Fosb* by bisulfite conversion, there was no effect of HSV-*Fosb*-ZFP35-G9a (**Fig. 1i**). Notably, the site targeted by ZFP35 coincides with a region in which we previously observed regulation of endogenous G9a binding in response to cocaine treatments[12], supporting the physiological relevance of *Fosb*-ZFP35-G9a action in regulating *Fosb* expression and the potential use of this tool for understanding mechanisms controlling *Fosb* expression *in vivo*.

Given that cocaine-induced ΔFosB protein accumulation contributes to the addiction phenotype, we sought to interfere with this physiological response by inducing H3K9me2 specifically at the *Fosb* locus (**Fig. 3**). Mice were injected with HSV-*Fosb*-ZFP35-G9a and HSV-*Fosb*-ZFP35-NFD in the right and left NAc, respectively, and then treated with repeated saline or cocaine (20 mg per kg of body weight) over a time course designed to coincide with HSV expression (72 h) while remaining sufficiently long enough to lead to FosB/ΔFosB protein accumulation in NAc (**Fig. 3a**). Immunohistochemical analysis using an antibody to FosB/ΔFosB revealed that, although cocaine increased the number of FosB-immunopositive NAc neurons by 39% in NAc infected with control virus, expression of HSV-*Fosb*-ZFP35-G9a blocked this induction (**Fig. 3b**,**c**). At this time point (7 d after HSV injection), HSV-mediated transgene expression had fully dissipated; thus, it was not possible to selectively examine the infected cells, which likely accounts for the fact that expression of FosB/ΔFosB in saline-treated mice was not affected by HSV-*Fosb*-ZFP35-G9a (**Fig. 3b**,**c**).

To further our understanding of cocaine-regulated *Fosb* expression, we sought to discover a molecular mechanism by which an increase in H3K9me2 solely at the *Fosb* promoter blocks cocaine induction of FosB/ΔFosB protein *in vivo*. We reasoned that this repressive histone modification might interfere with activation (that is, phosphorylation) of cAMP response element–binding protein (phospho-CREB(S133)) and/or serum response factor (phospho-SRF(S103)), both of which are required for *Fosb* induction in the NAc by repeated cocaine[32]. We injected mouse NAc with either control HSV or HSV-*Fosb*-ZFP35-G9a and then treated the animals with either repeated saline or cocaine (20 mg per kg). qChIP revealed that cocaine treatment resulted in a 3.9-fold enrichment of phospho-CREB at the *Fosb* promoter compared with saline-treated mice (**Fig. 3d**). This enrichment was blocked by NAc injection of HSV-*Fosb*-ZFP35-G9a (**Fig. 3d**). As previously demonstrated[32], cocaine had no effect on the enrichment of total CREB protein at the *Fosb* promoter, and HSV-*Fosb*-ZFP35-G9a did not alter levels of total CREB binding (**Fig. 3e**). Notably, cocaine treatment caused enrichment of phospho-SRF binding at the *Fosb* promoter, but there was only a modest effect of HSV-*Fosb*-ZFP35-G9a (**Fig. 3f**),

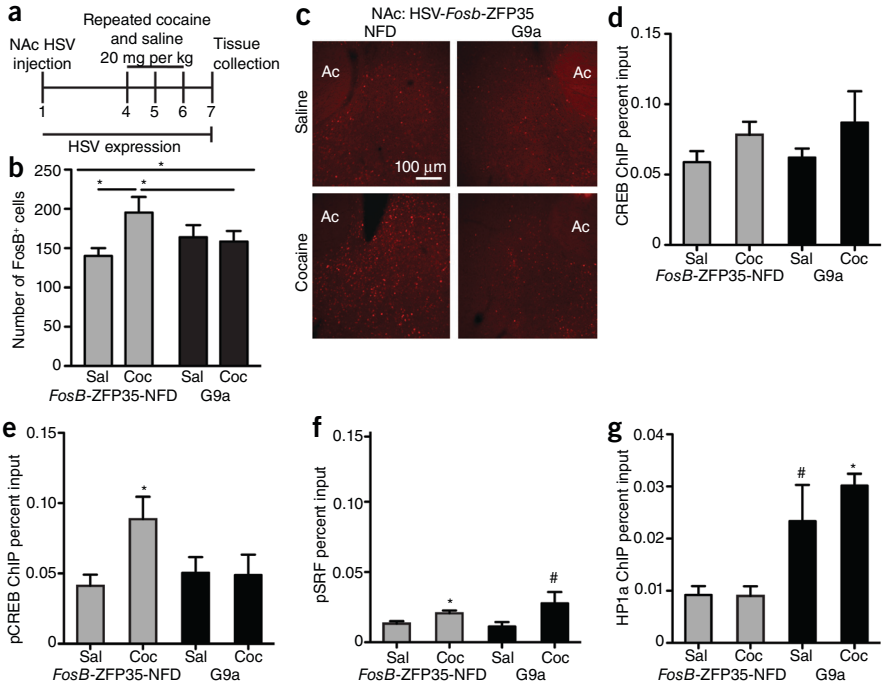

Figure 3 Cocaine induction of FosB/ΔFosB protein expression and endogenous transcription factor binding is blocked by HSV-*Fosb*-ZFP35-G9a in the NAc. (**a**) Mice were injected intra-NAc with HSV-*Fosb*-ZFP35-NFD or HSV-*Fosb*-ZFP35-G9a and treated with repeated cocaine (20 mg per kg) or saline. (**b**) Cocaine induction of FosB/ΔFosB$^+$ cells in the NAc is suppressed by *Fosb*-ZFP35-G9a (two-way ANOVA: interaction between virus (NFD, G9a) and drug (saline (sal), cocaine (coc)) ($F_{1,28} = 6.6$, $^*P = 0.016$, $n = 8$ mice per group); no main effects of virus ($F_{1,28} = 0.98$, $P = 0.330$, $n = 8$) or drug ($F_{1,28} = 1.18$, $P = 0.286$, $n = 8$) alone). Cocaine enhances FosB$^+$ cell levels in NFD-infected tissue ($t_{14} = 2.48$, $^*P = 0.027$, $n = 8$), but not G9a-infected tissue ($t_{14} = 1.20$, $P = 0.291$, $n = 8$). Among animals receiving cocaine, G9a repressed FosB/ΔFosB$^+$ cells ($t_{14} = 2.25$, $^*P = 0.041$, $n = 8$). (**c**) Representative images from mice infected with HSV-*Fosb*-ZFP35-NFD in the left hemisphere and HSV-*Fosb*-ZFP35-G9a into the right hemisphere. Ac, anterior commissure. (**d**) No change was observed in total CREB at the *Fosb* promoter after cocaine treatment in NAc injected with either virus (NFD, $t_{18} = 1.55$, $P = 0.138$, $n = 9, 11$; G9a, $t_{15} = 1.13$, $P = 0.274$; $n = 8, 9$). (**e**) Compared with saline, repeated cocaine treatment caused enrichment of phospho-CREB(S133) at the *Fosb* promoter in NAc injected with HSV-*Fosb*-ZFP35-NFD ($t_{17} = 2.38$, $^*P = 0.029$, $n = 9, 11$), but not with HSV-*Fosb*-ZFP-G9a ($t_{15} = 0.09$, $P = 0.932$, $n = 8, 9$). (**f**) Compared with saline, repeated cocaine treatment resulted in enrichment of phospho-SRF(S103) at the *Fosb* promoter in NAc injected with HSV-*Fosb*-ZFP35-NFD ($t_{1,6} = 2.7$, $^*P = 0.034$, $n = 4$, 4 ChiP samples) compared with repeated saline with only a modest effect of HSV-*Fosb*-ZFP-G9a in blocking this enrichment ($t_{(1,8)} = 1.9$, $^\#P = 0.097$; $n = 5, 5$). (**g**) NAc injection of HSV-*Fosb*-ZFP-G9a caused enrichment of HP1α at the *Fosb* promoter compared with HSV-*Fosb*-ZFP-NFD under cocaine conditions ($t_{1,7} = 1.24$, $^*P = 0.0002$, $n = 4, 5$) and a trend under saline treatment conditions ($t_{1,8} = 1.97$, $^\#P = 0.085$, $n = 4, 5$). Data are presented as mean ±s.e.m.

despite the close proximity of the CREB and SRF binding sites (**Fig. 1a**). We also examined the enrichment of HP1α at the *Fosb* promoter and found that, although cocaine did not regulate binding of this protein to *Fosb* in NAc, HSV-*Fosb*-ZFP35-G9a expression led to enrichment of HP1α in either the cocaine or saline context (**Fig. 3g**), as shown earlier (**Fig. 1h**). These data demonstrate that, in fully differentiated adult neurons *in vivo*, a primary increase in H3K9me2 at a given gene controls enrichment of an activated transcription factor at that gene and the gene's expression in response to an environmental stimulus.

Regulation of *Fosb* by transcription activator-like effectors

To gain a broader understanding of transcriptional regulation by engineered transcription factors, we targeted the *Fosb* gene with TALEs[17,33], a distinct type of designer DNA binding domain, as well as with a variety of transcriptional activators, including VP64, VP16 and 2xp65 (**Supplementary Fig. 3**). *Fosb* TALEs fused to the transactivator VP64 efficiently upregulated expression of *Fosb*/Δ*Fosb* when virally expressed in the NAc, whereas *Klf4*-TALE-VP64 had no effect (**Supplementary Fig. 3b**). Furthermore, VP16, VP64 and 2xp65 activated *Fosb*/Δ*Fosb* expression when fused to *Fosb*-ZFP35 and expressed in N2a cells (**Supplementary Fig. 3d**).

Such a comprehensive analysis demonstrated that engineered transcription factors are potent, bidirectional regulators of FosB/ΔFosB expression, yet we also found that their effect in cell culture was not always an accurate predictor of their function in brain. For example, *Fosb*-ZFP25-p65 robustly activated *Fosb*/Δ*Fosb* expression in N2a cells (**Supplementary Fig. 1**) but failed to activate transcription when expressed in NAc neurons *in vivo* (**Fig. 1d**). We also observed that several *Fosb*-ZFP-G9a constructs activated *Fosb* expression in N2a cells (**Supplementary Fig. 1**), but repressed expression in NAc neurons *in vivo* (**Fig. 1d**). To investigate a potential explanation for these discrepancies, we compared the expression level of ZFP constructs *in vitro* versus *in vivo* and found several orders of magnitude greater expression in N2a cells than in NAc (**Supplementary Fig. 4a**). However, titration of the amount of *Fosb*-ZFP35-G9a expressed in N2a cells affected the expression of Δ*Fosb*, but not *Fosb*, mRNA, indicating that ZFP expression levels account for only a part of its distinct function *in vitro* and *in vivo* (**Supplementary Fig. 4b**). An alternative explanation is provided by the fact that chromatin state is a major determinant of transcription factor binding and function and that such states differ between cell types[34,35]. These data underscore the importance of our approach in using an *in vivo* system to characterize engineered transcription factors as tools to study epigenetic mechanisms of gene regulation in reward regions of mammalian brain.

Regulation of reward behavior by *Fosb*-ZFPs

Having established a mechanism by which engineered transcription factors can specifically regulate ΔFosB expression *in vivo*, we next investigated their ability to modulate reward behaviors, starting with the regulation of cocaine action (**Fig. 4**). Mice were injected intra-NAc with HSV-*Fosb*-ZFP35, HSV-*Fosb*-TALE1 or control vectors and their locomotor activity was recorded over several days of cocaine treatment at either a sensitizing dose (10 mg per kg) or a subthreshold dose (5 mg per kg) that does not lead to locomotor sensitization in control animals (**Fig. 4a** and **Supplementary Fig. 3e**). We found that HSV-*Fosb*-ZFP35-G9a expression in NAc efficiently blocked cocaine locomotor sensitization (10 mg per kg; **Fig. 3c**), whereas both HSV-*Fosb*-ZFP35-p65 and HSV-TALE1-VP64 augmented the sensitizing effects of the drug,

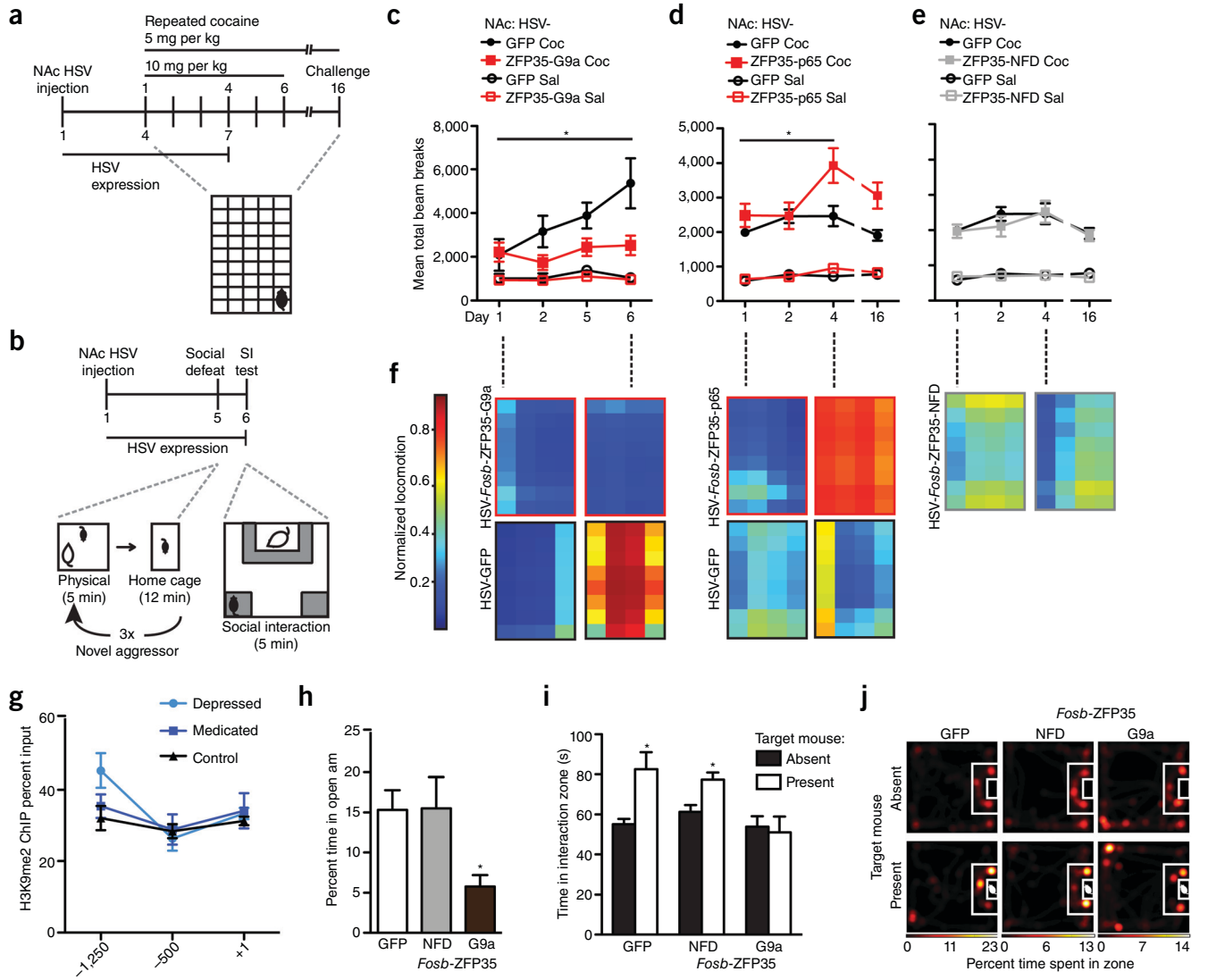

Figure 4 Engineered transcription factors bidirectionally modulate cocaine- and stress-evoked behaviors. (**a**) Locomotor activity was assessed during repeated cocaine exposure in mice injected intra-NAc with HSV-*Fosb*-ZFP35-G9a ($n = 7$), HSV-*Fosb*-ZFP35-p65 ($n = 9$), HSV-*Fosb*-ZFP35-NFD ($n = 9$) or control virus ($n = 5$ mice per group (10 mg per kg) or $n = 10$ (5 mg per kg)). (**b**) Social behavior was measured 24 h after subthreshold social defeat in mice injected with HSV-*Fosb*-ZFP35-G9a or control virus into the NAc. (**c**) At high doses of cocaine (10 mg per kg), locomotor behavior sensitized over time and this effect was blocked by HSV-*Fosb*-ZFP35-G9a in NAc. Repeated-measures ANOVA revealed an interaction between day, cocaine and virus ($F_{3,18} = 4.00$, $^*P = 0.024$) on locomotor behavior. Among cocaine-treated mice, there was a main effect of virus ($F_{1,10} = 8.81$, $P = 0.026$) and a trend for an interaction between virus and day ($F_{2,8} = 3.33$, $P = 0.077$) such that GFP locomotor behavior was enhanced above *Fosb*-ZFP35-G9a levels by treatment day 6 ($t_{1,10} = 2.61$, $P = 0.026$). (**d**) At low doses (5 mg per kg), cocaine-induced locomotor behavior sensitized over time with *Fosb*-ZFP35-p65 in NAc (repeated measures: interaction between day, treatment and virus, $F_{3,32} = 4.71$, $^*P = 0.008$). Among cocaine-treated mice, there was an interaction between virus and day ($F_{2,15} = 7.08$, $P = 0.003$) and a trend for a main effect of day among *Fosb*-ZFP35-p65 ($F_{1,32} = 2.85$, $P = 0.053$), but not *Fosb*-ZFP35-GFP cocaine-treated animals. Among cocaine-treated animals, *Fosb*-ZFP35-p65 enhanced locomotor behavior above *Fosb*-ZFP35-GFP levels by treatment day 4 ($t_{17} = 2.58$, $P = 0.020$) through day 16 ($t_{17} = 2.92$, $P = 0.009$). (**e**) NAc injection of HSV-*Fosb*-ZFP35-NFD, similar to controls, did not display cocaine locomotor sensitization to a low dose of cocaine. Repeated measures failed to find an interaction among day, treatment and virus ($F_{1,28} = 0.13$, $P = 0.944$). There was no effect of day among cocaine-treated mice ($F_{1,28} = 0.86$, $P = 0.471$). HSV-GFP data from **d** are shown. (**f**) Heat maps show representative locomotor data in the chamber for mice over the course of repeated cocaine exposure. (**g**) H3K9me2 was significantly enriched at –1,250 bp from the *Fosb* TSS in depressed humans ($t_{22} = 2.19$, $P = 0.040$, $n = 8$, 17 subjects per group) compared with levels in control subjects. (**h**) *Fosb*-ZFP35-G9a in the NAc reduced exploration of the open arm in the elevated plus maze compared with control virus ($t_{12} = 2.36$, $^*P = 0.036$, $n = 7$ mice per group). (**i**) HSV-*Fosb*-ZFP35-G9a in the NAc blocked increased exploration of a novel aggressor mouse after exposure to subthreshold social defeat, compared with control virus ($t_{12} = 3.1$, $^*P = 0.009$, $n = 7$ mice per group) with no effect of HSV-*Fosb*-ZFP35-NFD ($t_{12} = 3.2$, $^*P = 0.008$, $n = 7$). (**j**) Representative heat maps of social interaction after a subthreshold defeat stress showed a preference for the interaction zone when a target mouse was present for mice injected with control virus and HSV-*Fosb*-ZFP35-NFD, but not HSV-*Fosb*-ZFP35-G9a. Data are presented as mean ±s.e.m.

with no effect of HSV-*Fosb*-ZFP35-NFD (5 mg per kg; **Fig. 4d,e** and **Supplementary Fig. 3e**). None of the constructs affected baseline locomotor activity seen in the absence of cocaine compared with control virus (**Fig. 4c–e** and **Supplementary Fig. 3e**).

Recent evidence has also implicated a reduction of ΔFosB levels in the NAc in the etiology of depression in humans and in chronic stress models in rodents[8]. Indeed, we found that depressed human NAc exhibited a 37% enrichment of H3K9me2 at the *FOSB* promoter (**Fig. 3g**), specifically at a

site 1,200 bp upstream from the TSS, coincident with the site of greatest H3K9me2 enrichment at the *Fosb* promoter in mouse NAc (**Fig. 1g**). On the basis of these results, we examined the effect of artificially inducing H3K9me2 selectively at the *Fosb* gene in mouse NAc, thereby mimicking this single pathological histone modification in depressed humans. We relied on a variant of the chronic social defeat stress (CSDS) procedure, in which animals are subjected to a subthreshold social stress that has no effect on depression-related behaviors, such as social avoidance, in normal animals[36]. Mice were injected with HSV-*Fosb*-ZFP-G9a into NAc, allowed to recover for 5 d, and then exposed to an aggressor for three bouts of 5 min each (**Fig. 4b**). In contrast with control virus, mice that were infected with HSV-*Fosb*-ZFP35-G9a showed reduced social interaction when tested 24 h after the aggressive encounter, a pro-depression–like behavioral response (**Fig. 4i**). Furthermore, we found that these mice spent less time exploring the open arms in the elevated plus maze, indicative of increased anxiety-related behavior (**Fig. 3h**). Thus, mimicking a single HPTM abnormality seen at a single gene in the NAc of depressed humans is sufficient to promote behavioral susceptibility to stress.

DISCUSSION

We used engineered transcription factors to site-selectively remodel chromatin in a discrete brain region to control both the molecular and behavioral effects of drug and stress exposure. We targeted the *Fosb* gene because of its known role in the pathophysiology of drug addiction and depression in both rodents and humans, which has been linked to epigenetic remodeling at this locus. Specifically, drug-induced activation of *Fosb* is correlated with increased histone acetylation and decreased histone methylation at its promoter, yet it has not previously been possible to elucidate the functional relevance of such changes as a result of the genome-wide context in which they occur. To overcome this limitation, we designed a suite of engineered transcription factors that target the *Fosb* locus and applied them to the expression of *Fosb*/Δ*Fosb* under both basal and cocaine-induced conditions. We found that *Fosb*-ZFPs and *Fosb*-TALEs fused to the transcriptional activators p65 or VP64, respectively, activated *Fosb*/Δ*Fosb* expression in both cultured cells and when virally expressed in NAc. NAc expression of *Fosb*-ZFP35-p65 induced histone acetylation across the *Fosb* promoter, a modification that has been implicated in cocaine-induced activation of this locus[1]. We found that acetylation of *Fosb* by *Fosb*-ZFP35-p65 was sufficient to enhance the sensitizing effects of cocaine, indicating that ZFP-induced acetylation may act synergistically with cocaine-activation of this gene to produce an enhanced behavioral response. In a complementary procedure, we found that histone methylation by *Fosb*-ZFP35-G9a was sufficient to repress basal expression of *Fosb*/Δ*Fosb in vivo* and block cocaine locomotor sensitization. These results represent, to the best of our knowledge, the first demonstration of ZFP-induced chromatin modifications *in vivo* and the first use of engineered transcription factors to elucidate transcriptional dysregulation underlying neuropsychiatric disease.

We included numerous control constructs in our study to rule out the effects of stoichiometric interference by ZFPs in the transcription of *Fosb*. We found that *Fosb*-ZFP35 without a functional domain did not affect *Fosb*/Δ*Fosb* expression or chromatin modification in either the basal or cocaine contexts. To further establish the specificity of our engineered transcription factors in targeting *Fosb* selectively, we analyzed the regulation of 28 potential off-target binding motifs *in vivo*, each of which differs from the ZFP35 binding site by one to three nucleotides, and found no transcriptional regulation of their associated genes by *Fosb*-ZFP35-p65 or *Fosb*-ZFP35-G9a. In addition, we found no enrichment of H3K9me2 at six of these sites examined after expression of *Fosb*-ZFP35-G9a. Our results are consistent with a small number of *in vitro* studies that have examined ZFP or TALE specificity and concluded that there is little to no genome-wide transcription regulation by gene-targeted engineered transcription factors[17,37,38]. Our data are, to the best of our knowledge, the first to demonstrate the functional specificity of engineered transcription factors in neurons *in vivo*, thereby greatly enhancing their use for the study of the epigenetic underpinnings of neuropsychiatric disease.

Previous studies have demonstrated the dynamic regulation of histone methylation by both chronic cocaine and stress[11,12]. In particular, repeated cocaine treatment reduces G9a expression and the enrichment of H3K9me2 in the NAc, resulting in derepression at hundreds of genes, including *Fosb*; viral overexpression of G9a in NAc increases H3K9me2 at *Fosb*, represses ΔFosB expression and inhibits cocaine reward behavior[12]. Our results improve on this previous approach by targeting G9a specifically to the *Fosb* gene, thereby arguing against effects of G9a across the genome and directly implicating G9a-induced H3K9me2 at *Fosb* in the specific mechanism of *Fosb* gene repression.

Histone methylation is thought to repress gene expression via the recruitment of additional methyltransferases and HP1, which can lead to the formation of silent heterochromatin[30,39]. We found that *Fosb*-ZFP35-G9a induced H3K9me2 enrichment across the *Fosb* promoter, up to 1,000 bp upstream from the ZFP recognition motif. This site, 1,250 bp upstream from the *Fosb* TSS, showed the greatest basal enrichment in H3K9me2 in both mouse and human NAc, and we found that, following ZFP-induced H3K9me2, binding of HP1α was increased only at this location. In non-nervous tissues, repression by H3K9me2 often involves not only the recruitment of HP1, but also generation of H3K9me3, and can spread to adjacent genomic regions[40,41]. Given the widespread methylation induced by *Fosb*-ZFP35-G9a, we investigated H3K9me3 binding across the *Fosb* promoter and found, to our surprise, that this modification was depleted at the site of HP1α and H3K9me2 co-enrichment, with no regulation elsewhere in the *Fosb* promoter. We also measured DNA methylation at three CpGs located adjacent to this region, as DNA methyltransferase is also often recruited by HP1 and H3K9me2/3 (ref. 42), but did not find regulation of DNA methylation coincident with induced H3K9me2. Taken together, our results demonstrate a causal mechanism of gene repression at a euchromatic locus that is initiated by G9a recruitment, leading to enrichment of H3K9me2 and binding of HP1α, a mechanism of G9a/H3K9me2 action in fully differentiated adult neurons *in vivo* that differs from models based on other systems.

We next investigated a potential mechanism by which ZFP-induced H3K9me2 enrichment blocks cocaine-evoked *Fosb* expression in NAc. We found that this manipulation was sufficient to prevent the increase in phospho-CREB at the *Fosb* promoter, which is required for cocaine-evoked *Fosb*/Δ*Fosb* expression[32] and is known to be important for cellular and behavioral plasticity relevant to drug exposure[8]. Our results revealed no effect of H3K9me2 on the binding of total CREB or of phospho-SRF, indicating a specific action of H3K9me2 in preventing the phosphorylation of CREB already bound to *Fosb*. These results provide, to the best of our knowledge, the first direct evidence of a drug-evoked histone modification regulating gene expression by controlling transcription factor activity. Further studies will be needed to shed light on the mechanism by which H3K9me2 enrichment prevents CREB phosphorylation, especially given the ~1,000-bp distance between their binding sites.

Fosb has also been implicated in the cellular and behavioral correlates of stress and depression. In particular, previous studies have demonstrated that *Fosb*/Δ*Fosb* expression in the NAc is deficient in the social isolation model of depression in mice and in this region of postmortem depressed patients, and that increased *Fosb*/Δ*Fosb* expression in NAc protects animals from the deleterious effects of chronic stress[8]. To complement these data, we found that H3K9me2 was enriched at the *FOSB* promoter in NAc of depressed patients relative to controls, implicating this repressive epigenetic modification in the repression of *FOSB* in this population. Indeed,

we found that ZFP-induced enrichment of H3K9me2 at *Fosb* in mouse NAc was not only sufficient to reduce *Fosb/ΔFosb* expression, but also induced a pro-depressive state, as manifested by depression- and anxiety-like behaviors after social stress. These data suggest a causal epigenetic mechanism for *Fosb* repression in the pathophysiology of depression.

In summary, we found that histone methylation or acetylation *per se* at the *Fosb* locus in the NAc is sufficient to dynamically regulate gene expression at this locus and thereby control the behavioral effects of cocaine or stress exposure. The ability to site-specifically modify chromatin enabled us to model a pathological epigenetic marker of human addiction and depression and observe the effects on drug and stress susceptibility in mice. Our findings also suggest that a primary change in H3K9me2 is sufficient to drive downstream changes in transcription factor binding and gene expression, which is in contrast with current models of HPTMs occurring mostly secondarily to alterations in transcription factors. By expanding this approach to target additional genes and HPTMs regulated by emotional stimuli, it will be possible to gradually build a detailed understanding of the epigenetic basis of addiction and depression.

METHODS

Methods and any associated references are available in the online version of the paper.

Note: Any Supplementary Information and Source Data files are available in the online version of the paper.

ACKNOWLEDGMENTS

The authors wish to thank G. Stuber and R. Ung for their help in generating social interaction heat maps. This work was supported by grants from the National Institute on Drug Abuse (E.A.H. and E.J.N.), the National Institute of Mental Health and the Hope for Depression Research Foundation (E.J.N.).

AUTHOR CONTRIBUTIONS

E.A.H. designed and executed the biochemical, molecular and behavioral experiments (viral packaging constructs, qRT-PCR expression analysis, chromatin immunoprecipitation (mouse and human), immunohistochemical preparation and behavioral assays). H.M.C. and H.S. generated viral packaging constructs, conducted expression analysis and prepared chromatin. C.J.P. and S.A.G. analyzed immunohistochemical data. N.S. and L.S. conducted genome-wide sequence analysis. J.F. and E.A.H. performed DNA methylation sequencing. S.A.G. and S.J.R. generated human chromatin. E.A.H., H.M.C., H.S., J.J.W., M.M.-R., D.F. and M.-H.H. performed stereotaxic mouse surgery. J.P.H. generated mouse locomotor heat maps. C.S.T. prepared human postmortem brain tissue. R.L.N. generated HSV viral vectors. H.S.Z. generated the G9a catalytic domain construct. S.K., M.A.G. and C.N. generated the ZFP constructs. F.Z. generated the TALE constructs. C.J.P., E.A.H. and H.M.C. analyzed the data conducted statistical analyses. E.A.H. and E.J.N. discussed the data and wrote the manuscript.

COMPETING FINANCIAL INTERESTS

The authors declare no competing financial interests.

1. Renthal, W. *et al.* Genome-wide analysis of chromatin regulation by cocaine reveals a role for sirtuins. *Neuron* **62**, 335–348 (2009).
2. Kennedy, P.J. *et al.* Class I HDAC inhibition blocks cocaine-induced plasticity by targeted changes in histone methylation. *Nat. Neurosci.* **16**, 434–440 (2013).
3. Malvaez, M., Mhillaj, E., Matheos, D.P., Palmery, M. & Wood, M.A. CBP in the nucleus accumbens regulates cocaine-induced histone acetylation and is critical for cocaine-associated behaviors. *J. Neurosci.* **31**, 16941–16948 (2011).
4. Robison, A.J. & Nestler, E.J. Transcriptional and epigenetic mechanisms of addiction. *Nat. Rev. Neurosci.* **12**, 623–637 (2011).
5. Feng, J. *et al.* Chronic cocaine-regulated epigenomic changes in mouse nucleus accumbens. *Genome Biol.* **15**, R65 (2014).
6. Kumar, A. *et al.* SOM Chromatin remodeling is a key mechanism underlying cocaine-induced plasticity in striatum. *Neuron* **48**, 303–314 (2005).
7. Kelz, M.B. *et al.* Expression of the transcription factor ΔFosB in the brain controls sensitivity to cocaine. *Nature* **401**, 272–276 (1999).
8. Vialou, V. *et al.* ΔFosB in brain reward circuits mediates resilience to stress and antidepressant responses. *Nat. Neurosci.* **13**, 745–752 (2010).
9. Robison, A.J. *et al.* Behavioral and structural responses to chronic cocaine require a feedforward loop involving ΔFosB and calcium/calmodulin-dependent protein kinase II in the nucleus accumbens shell. *J. Neurosci.* **33**, 4295–4307 (2013).
10. Maze, I. *et al.* Cocaine dynamically regulates heterochromatin and repetitive element unsilencing in nucleus accumbens. *Proc. Natl. Acad. Sci. USA* **108**, 3035–3040 (2011).
11. Covington, H.E. *et al.* A role for repressive histone methylation in cocaine-induced vulnerability to stress. *Neuron* **71**, 656–670 (2011).
12. Maze, I. *et al.* Essential role of the histone methyltransferase G9a in cocaine-induced plasticity. *Science* **327**, 213–216 (2010).
13. Sun, H. *et al.* Morphine epigenomically regulates behavior through alterations in histone H3 lysine 9 dimethylation in the nucleus accumbens. *J. Neurosci.* **32**, 17454–17464 (2012).
14. Snowden, A.W., Gregory, P.D., Case, C.C. & Pabo, C.O. Gene-specific targeting of H3K9 methylation is sufficient for initiating repression *in vivo*. *Curr. Biol.* **12,** 2159–2166 (2002).
15. Sanjana, N.E. *et al.* A transcription activator-like effector toolbox for genome engineering. *Nat. Protoc.* **7**, 171–192 (2012).
16. Konermann, S. *et al.* Optical control of mammalian endogenous transcription and epigenetic states. *Nature* **500**, 472–476 (2013).
17. Mendenhall, E.M. *et al.* Locus-specific editing of histone modifications at endogenous enhancers. *Nat. Biotechnol.* **31**, 1133–1136 (2013).
18. Laganiere, J. *et al.* An engineered zinc finger protein activator of the endogenous glial cell line-derived neurotrophic factor gene provides functional neuroprotection in a rat model of Parkinson's disease. *J. Neurosci.* **30**, 16469–16474 (2010).
19. Beerli, R.R. & Barbas, C.F. Engineering polydactyl zinc-finger transcription factors. *Nat. Biotechnol.* **20**, 135–141 (2002).
20. Gerritsen, M.E. *et al.* CREB-binding protein/p300 are transcriptional coactivators of p65. *Proc. Natl. Acad. Sci. USA* **94**, 2927–2932 (1997).
21. Covington, H.E. *et al.* Antidepressant actions of histone deacetylase inhibitors. *J. Neurosci.* **29**, 11451–11460 (2009).
22. Malvaez, M., Mhillaj, E., Matheos, D.P., Palmery, M. & Wood, M.A. CBP in the nucleus accumbens regulates cocaine-induced histone acetylation and is critical for cocaine-associated behaviors. *J. Neurosci.* **31**, 16941–16948 (2011).
23. Kennedy, P.J. *et al.* Class I HDAC inhibition blocks cocaine-induced plasticity by targeted changes in histone methylation. *Nat. Neurosci.* **16**, 434–440 (2013).
24. Kumar, A. *et al.* Chromatin remodeling is a key mechanism underlying cocaine-induced plasticity in striatum. *Neuron* **48**, 303–314 (2005).
25. Peixoto, L. & Abel, T. The role of histone acetylation in memory formation and cognitive impairments. *Neuropsychopharmacology* **38**, 62–76 (2013).
26. Rogge, G.A., Singh, H., Dang, R. & Wood, M.A. HDAC3 is a negative regulator of cocaine-context-associated memory formation. *J. Neurosci.* **33**, 6623–6632 (2013).
27. Rea, S. *et al.* Regulation of chromatin structure by site-specific histone H3 methyltransferases. *Nature* **406**, 593–599 (2000).
28. Garriga-Canut, M. *et al.* Synthetic zinc finger repressors reduce mutant huntingtin expression in the brain of R6/2 mice. *Proc. Natl. Acad. Sci. USA* **109**, E3136–E3145 (2012).
29. Smith, A.E., Hurd, P.J., Bannister, A.J., Kouzarides, T. & Ford, K.G. Heritable gene repression through the action of a directed DNA methyltransferase at a chromosomal locus. *J. Biol. Chem.* **283**, 9878–9885 (2008).
30. Fritsch, L. *et al.* A subset of the histone H3 lysine 9 methyltransferases Suv39h1, G9a, GLP and SETDB1 participate in a multimeric complex. *Mol. Cell* **37**, 46–56 (2010).
31. Filion, G. J. & van Steensel, B. Reassessing the abundance of H3K9me2 chromatin domains in embryonic stem cells. *Nat. Genet.* **42**, 4 (2010).
32. Vialou, V. *et al.* Serum response factor and cAMP response element binding protein are both required for cocaine induction of FosB. *J. Neurosci.* **32**, 7577–7584 (2012).
33. Zhang, F. *et al.* Efficient construction of sequence-specific TAL effectors for modulating mammalian transcription. *Nat. Biotechnol.* **29**, 149–153 (2011).
34. Maniatis, T., Goodbourn, S. & Fischer, J.A. Regulation of inducible and tissue-specific gene expression. *Science* **236**, 1237–1245 (1987).
35. Ernst, J. & Kellis, M. Interplay between chromatin state, regulator binding, and regulatory motifs in six human cell types. *Genome Res.* **23**, 1142–1154 (2013).
36. Chaudhury, D. *et al.* Rapid regulation of depression-related behaviors by control of midbrain dopamine neurons. *Nature* **493**, 532–536 (2013).
37. Smith, D.J. & Konarska, M.M. A critical assessment of the utility of protein-free splicing systems. *RNA* **15**, 1–3 (2009).
38. Grimmer, M.R. *et al.* Analysis of an artificial zinc finger epigenetic modulator: widespread binding but limited regulation. *Nucleic Acids Res.* **42**, 10856–10868 (2014).
39. Kouzarides, T. Chromatin modifications and their function. *Cell* **128**, 693–705 (2007).
40. Lachner, M., O'Carroll, D., Rea, S., Mechtler, K. & Jenuwein, T. Methylation of histone H3 lysine 9 creates a binding site for HP1 proteins. *Nature* **410**, 116–120 (2001).
41. Hathaway, N.A. *et al.* Dynamics and memory of heterochromatin in living cells. *Cell* **149**, 1447–1460 (2012).
42. Cedar, H. & Bergman, Y. Linking DNA methylation and histone modification: patterns and paradigms. *Nat. Rev. Genet.* **10**, 295–304 (2009).
43. Paxinos, G. & Franklin, K.B.J. *The Mouse Brain in Stereotaxic Coordinates* (Academic Press, 2012).

ONLINE METHODS

Mice and treatments. Male 7–8-week-old C57BL/6J mice and 6-month-old CD1 retired breeders (CD1 aggressor) were housed at 22–25 °C in a 12-h light/dark cycle and provided food and water *ad libitum*. Mice were housed five per cage and habituated in our facility for at least 1 week before experimentation, and all tests were conducted during the light cycle. Members of the same cage were randomly assigned to different experimental groups for behavioral studies and the order of testing was distributed across groups. Wherever possible, the experimenter conducting the data analysis was blind to treatment conditions of the animals. All experiments were conducted in accordance with the guidelines of the Institutional Animal Care and Use Committee at Mount Sinai. Group size determination was based on published protocols for the behavioral procedure in use; no statistical test was used to predetermine sample size. For repeated cocaine experiments (immunohistochemistry, ChIP), animals received daily injections of either saline (five treatments of saline, intraperitoneal) or saline followed by cocaine (one treatment of saline, four treatments of cocaine, 20 mg per kg, intraperitoneal) and were killed 24 h after the last injection. Sample size was determined based on empirical data in preliminary experiments and published protocols.

Transcription factor engineering. All ZFPs were manufactured by the CompoZr ZFN Operations Group at Sigma-Aldrich Biotechnology and cloned in frame N-terminal to the activation or repression domain. The ZFPs recognize the following unique 18–20-bp motifs in the *Fosb* promoter: ZFP1, TCCGTGACAAAGCTAGTGG; ZFP14, ACCTTCTCCAACCCGGGT; ZFP25, CAACAGCGGGCGCGCGCAG; ZFP29, CCAAACAAACACTGGGCCGC; ZFP31,GGCCGCGCTGGCCGAGCTCC; ZFP35, GATCCCCTCCCGCGAAGCC; ZFP54, TGCGGGTGACGCAAGCGCG; ZFP61, GCCGGGGACACGCGGAGCC; *Klf4* promoter, GTGACCCGCGCCCATGGCC. All TALE constructs were generated as described previously[15]. Briefly, TALE binding sites, 18-nucleotide targets with T as the first base, were selected from the promoter region of *Fosb*. All TALE repeat arrays were constructed using modular assembly followed by insertion into cloning backbones containing the non-repetitive TALE capping regions and the VP64 transcription activator. The identities of repeat variable diresidues (RVDs) in each TALE repeat array are as follows (name, target site (5′ to 3′), repeat array RVDs) or published[33]: *Fosb*-TALE1, TCCCCTCCCGCGAAGCCC, HD-HD-HD-HD-NG-HD-HD-HD-NN-HD-NN-HI-HI-NN-HD-HD-HD; *Fosb*-TALE2, TCACCCGCAACTCCATGC, HD-NI-HD-HD-HD-NN-HD-NI-NI-HD-NG-HD-HD-NI-NG-NN-HD; *Fosb*-TALE3, TACGCCGGGGACACGCGG, NI-HD-NN-HD-HD-NN-NN-NN-NN-NI-HD-NI-HD-NN-HD-NN-NN.

Bioinformatics. Bowtie was used to align FosB-ZFP35 motif to mouse genome (mm9)[44], and three mismatches at maximum was allowed (parameter: -v 3). Then, region_analysis.pl, a genome annotation utility in diffReps package[45], was applied to annotate the hit regions with RefSeq database. Only the hits within 3 kb to TSSs were subject to further validation.

N2a transfection and RNA isolation. Neuro2a cells (ATCC CCL-131; manufacturer's authentication available online) were cultured and transfected with 400 ng of plasmid DNA using Effectene reagent (Qiagen), and RNA was isolated using the RNeasy Mini Kit (Qiagen) according to the manufacturer's instructions. qPCR and data analysis were performed as described[11], using the primers listed in **Supplementary Table 1**. Data were analyzed by comparing C(t) values of the experimental construct with mock-transfected cells using the ΔΔC(t) method.

Viral-mediated gene transfer. Mice were anesthetized with a mixture of ketamine (100 mg per kg) and xylazine (10 mg per kg) and prepared for stereotaxic surgery. 33 gauge syringe needles (Hamilton) were used to bilaterally infuse 0.5–1.0 µl of virus into NAc at a rate of 0.1 µl min^{-1} at 1.6 mm A/P, +1.5 mm lateral and 4.4 mm D/V from Bregma. We used bicistronic p1005 HSV vectors expressing GFP alone or GFP plus *Fosb*-ZFP or *Fosb*-TALE. In this system, GFP expression is driven by a cytomegalovirus (CMV) promoter, whereas the select gene of interest is driven by the IE4/5 promoter[12]. As with other HSV vectors, we detected no change in neuronal viability with any of the vectors that we used.

NAc RNA isolation and qRT-PCR. 72 h after viral infection, when transgene expression was maximal, mice were rapidly decapitated and brains were removed and placed on ice. A fluorescence microscope (Leica) was used to visualize accurate NAc targeting of GFP-expressing virus and to accurately dissect only infected tissue. Dissections of NAc were taken with a 1-mm aluminum micropunch (Harris) and quickly frozen on dry ice until RNA was extracted. RNA isolation, qPCR and data analysis were performed as described[11], using the primers listed in **Supplementary Table 2**. Data were analyzed by comparing C(t) values of the experimental virus with control virus using the ΔΔC(t) method.

Western blotting. Frozen NAc tissue was homogenized in 30 µl of RIPA buffer containing 10 mM Tris, 150 mM NaCl, 1 mM EDTA, 0.1% SDS, 1% Triton X-100, 1% sodium deoxycholate and protease inhibitors (Roche) using an ultrasonic processor (Cole Parmer). Protein concentrations were determined using a DC protein assay (Bio-Rad), and 50 µg of protein were loaded onto 4–15% gradient Tris-HCl polyacrylamide gels for electrophoresis fractionation (Bio-Rad). Proteins were transferred to nitrocellulose membranes, blocked with Odyssey blocking buffer (Li-Cor) and incubated overnight at 4 °C with primary antibodies (FosB/ΔFosB, 1:500, Cell signaling 2551 (ref. 12); H3K9me2, 1:500, Abcam ab1220)[12] in Odyssey blocking buffer. After thorough washing with 1× Tris-buffered saline plus 0.1% Tween-20 (vol/vol), membranes were incubated with IRDye secondary antibodies (1:5,000 to 1:10,000, Li-Cor, 926-32213) dissolved in Odyssey blocking buffer for 1 h at 22–25 °C. For analysis, the blots were imaged with the Odyssey Infrared Imaging system (Li-Cor) and quantified by densitometry using ImageJ (US National Institutes of Health). The amount of protein blotted onto each lane was normalized to levels of actin (MP BioMedicals Clone C4). Representative image and data shown are from one experiment of two biological replicate experiments using two animal cohorts.

Immunohistochemistry, imaging and cell counting. Adult males were terminally anesthetized (chloral hydrate) and transcardially perfused with phosphate-buffered salien (PBS) followed by 4% paraformaldehyde (wt/vol). Brains were then post-fixed overnight in 4% paraformaldehyde at 4 °C, cryoprotected in 30% sucrose (wt/vol) at 4 °C until isotonic and stored at –80 °C. 35-µm coronal sections were sliced on a freezing microtome. Striatal sections were washed in PBS and blocked with 3% normal donkey serum (vol/vol, NDS) before incubating in primary antibody (rabbit antibody to FosB, 1:1,000, Santa Cruz Biotechnology sc-48 (ref. 46); rabbit antibody to DARPP32, 1:1,000, AbCam ab40801 (ref. 47); mouse antibody to NeuN, 1:10,000, Millipore MAB377 (refs. 46,48); chicken antibody to GFP, 1:8,000, Aves Labs GFP 10-10)[12] in 0.1% Triton X-100, 3% NDS and PBS at 4 °C overnight. Sections were then washed in PBS, incubated in secondary antibody (Cy3 donkey antibody toRabbit, 1:500, Jackson ImmunoResearch 711-165-152; Cy2 donkey antibody to chicken, 1:500, Jackson ImmunoResearch 103-225-155; Cy3 donkey antibody to mouse, 1:500, Jackson ImmunoResearch 715-165-150) in 0.1% Tween-20 and PBS, washed and mounted on poly-L-lysine–coated slides. Slides were washed briefly in 75% ethanol, dried and coverslipped with ProLong Gold anti-fade with DAPI (Life Technologies). Slides were stored in a light-proof box at 4 °C before and after imaging. Slides were imaged on an Axio Observer Inverted Microscope (Zeiss) fitted with fluorescent filters. For each animal, 4–8 sections along the A-P axis of the NAc were imaged at 20× magnification (AxioVision imaging software, Zeiss) by an observer blind to conditions. For anatomical consistency, images included a portion of the anterior commissure as a marker of the NAc. Images were taken simultaneously for DAPI, GFP and FosB (Cy3). Adjustments were made as necessary to accurately capture fluorescent intensity. Analysis of $FosB^+$ cells was performed using ImageJ. In the red channel, threshold was adjusted to accurately count moderate- to highly expressing $FosB^+$ cells. An elliptical of a constant size selected a region of interest through the core and shell of the NAc, and particles were analyzed (size, 15–175; circularity, 0.01–1) for each image. Representative image and data shown are from one experiment of two technical replicate experiments, in which sections from the same cohort of animals were subject to immunohistochemical analysis.

ChIP. ChIP was performed on bilateral NAc 15-gauge punches pooled from 4–5 mice 72 h after viral infection or 24 h after the last drug treatment, and dissected as described above, or 5×10^6 N2a cells 48 h after transfection. Chromatin was prepared as described previously[1] and sheared using a diogenode bioruptor XL at high sonication intensity for 30 s on/ 30 s off for either 25 min twice. Fragment size was verified with an Agilent 2100 bioanalyzer at 150–300 bp or 1,000–3,000 bp respectively. Sheared chromatin was incubated overnight with the following

antibodies previously bound to magnetic beads (Dynabeads M-280, Life Technologies): antibody to H3K9me2 (AbCam ab1220)[12], antibody to H3K27me3 (AbCam ab6002)[5], antibody to H3K4me3 (EMD Millipore 17-614)[5], antibody to H3K9/14ac (EMD Millipore 17-615)[1], antibody to H3K9me3 (EMD Millipore 07-442)[49], antibody to HP1α (EMD Millipore 05-689)[50], antibody to CREB (EMD Millipore 17-600)[32], antibody to phospho-CREB (EMD Millipore 17-10131)[32], antibody to phospho-SRF (AbCam ab53130). After reverse cross-linking and DNA purification (Qiagen Spin Column), binding to the *Fosb* promoter was determined by qRT-PCR using the primers listed in **Supplementary Table 2**.

DNA methylation. NAc tissue from three each of HSV-*Fosb*-ZFP35-NFD and HSV-*Fosb*-ZFP35-G9a viral injected animals was collected 4 d after surgery. Genomic DNA was isolated following standard protocol and treated with sodium bisulfite using Zymo EZ DNA Methylation kit. PCR was run with a primer pair (**Supplementary Table 1**) flanking a region (873–1,192 bp) upstream from the *Fosb* TSS. TOPO cloning was then performed following the manufacturer's instructions (Invitrogen). Minipreps were prepared and sequenced by Sanger sequencing (Macrogen).

Locomotor sensitization. Locomotor sensitization was measured per published protocols[7] with minor modifications. Activity was assessed in the x and y planes for horizontal ambulations in a 75-cm^2 chambers using Ethovision XT (Noldus). On each day of sensitization, mice were injected with saline and analyzed for 10–15 min, then immediately injected with cocaine (5 or 10 mg per kg) and analyzed for 45–60 min. In some cases, locomotor activity was measured 7 d after the last cocaine injection after mice were given a challenge injection of cocaine (5 mg per kg). Heat map color scales were generated by pooling individual pixel values across animals and treatments. Each animal's pixel values were computed from raw x- and y-beam break counts normalized to that animal's total count. The pairwise summation of 4 x- and 8 y-beam break counts resulted in 32 pixel values for each animal; each value was divisively normalized by the total sum of the 12 beam break counts and rounded to the nearest integer. Pixel values from all animals in a given plot were then pooled, and the number of unique integers in the pool determined the number of colors comprising a scale starting with dark blue, ranging through blue, cyan, green, yellow and red, and ending with dark red. Calculations and image generation were performed using MATLAB R2012b (MathWorks). Representative images show the locomotor activity of one animal in each group, selected as that which displayed total locomotor activity closest to the mean on day 1 of the experiment.

Subthreshold social defeat and social interaction test. This procedure is used to detect the mechanisms that promote a depression-like phenotype[36]. Male C57BL/6J mice were exposed to a novel CD1 male aggressor for 5 min, 3 times with 15-min intervals between each exposure. A social interaction test was performed 24 h later. For this test, the subject is placed in an open field arena divided into an interaction zone and two opposing corner zones. A social target (novel CD1 mouse) is placed in a metal mesh-plastic box in the interaction zone, which allows sensory, but not physical, interaction. Ethovision XT (Noldus) tracking software was used to measure the duration (s) the subject mouse spent in the interaction zone with and without the target CD1 present (2.5 min). Heat maps and post-acquisition processing were conducted in MATLAB (MathWorks) according to published protocols[51]. Representative images show the locomotor activity of one animal in each group from a single experiment. This experiment was repeated twice with separate animal cohorts.

Human postmortem brain tissue. Human postmortem brain tissue was obtained from the Dallas Brain Collection (DBC), where tissue is collected from the Dallas Medical Examiner's Office and the UT Southwestern Tissue Transplant Program after consent from the next of kin. Tissue was analyzed from 9 depressed patients (5 male, 4 female; age 44 ± 7, postmortem interval (PMI) 15 ± 2) and 18 controls (15 male, 3 female; age 51 ± 3; PMI 16 ± 1). The UT Southwestern Institutional Review Board reviewed and approved the collection of this tissue for research use. A direct informant interview was carried out for each depression sample at a later date, where information regarding the individual's illness was documented; a consensus diagnosis of major depressive disorder was made by psychiatrists using DSM-IV criteria. None of the samples included in the study had blood toxicology screens positive for drugs of abuse, alcohol or prescription drugs, including antidepressants. NAc dissection, tissue processing and chromatin preparation were performed as reported previously[52]. qChIP was performed using antibody to H3K9me2 antibody (ab1220, AbCam) previously bound to magnetic beads (Dynabeads M-280, Life Technologies). Analysis of relative enrichment was performed using qRT-PCR as described.

Statistics. The appropriate statistical test was determined based on the number of comparisons being done. Student's *t* tests were used for comparison of two groups, in the analysis of qRT-PCR, qChIP and social interaction data. One-way ANOVA was used for analysis of three or more experimental groups, with a Bonferroni correction test *post hoc*, when appropriate, in the analysis of mouse locomotor data. Main and interaction effects were considered significant at $P < 0.05$. Data are expressed as mean ± s.e.m. The Grubbs test was used when appropriate to identify outliers. F tests of variance were conducted on all data sets to ensure that the data followed a normal distribution. All experiments were carried out one to three times, and data replication was observed in instances of repeated experiments. Experimental sample sizes as indicated in the figure legends were determined to give the reported s.e.m. values that were sufficiently low to allow meaningful interpretation of the data.

A **Supplementary Methods Checklist** is available.

44. Langmead, B., Trapnell, C., Pop, M. & Salzberg, S.L. Ultrafast and memory-efficient alignment of short DNA sequences to the human genome. *Genome Biol.* **10**, R25 (2009).
45. Shen, L. *et al.* diffReps: detecting differential chromatin modification sites from ChIP-seq data with biological replicates. *PLoS ONE* **8**, e65598 (2013).
46. Lobo, M.K. *et al.* ΔFosB induction in striatal medium spiny neuron subtypes in response to chronic pharmacological, emotional and optogenetic stimuli. *J. Neurosci.* **33**, 18381–18395 (2013).
47. Becker, A. *et al.* Glutaminyl cyclase-mediated toxicity of pyroglutamate-beta amyloid induces striatal neurodegeneration. *BMC Neurosci.* **14**, 108 (2013).
48. US National Research Council Committee on Guidelines for the Use of Animals in Neuroscience and Behavioral Research. *Guidelines for the Care and Use of Mammals in Neuroscience and Behavioral Research* (National Academies Press (US), 2003).
49. Maze, I. *et al.* Cocaine dynamically regulates heterochromatin and repetitive element unsilencing in nucleus accumbens. *Proc. Natl. Acad. Sci. USA* **108**, 3035–3040 (2011).
50. Allan, R.S. *et al.* An epigenetic silencing pathway controlling T helper 2 cell lineage commitment. *Nature* **487**, 249–253 (2012).
51. Jennings, J.H. *et al.* Distinct extended amygdala circuits for divergent motivational states. *Nature* **496**, 224–228 (2013).
52. Golden, S.A. *et al.* Epigenetic regulation of RAC1 induces synaptic remodeling in stress disorders and depression. *Nat. Med.* **19**, 337–344 (2013).

doi:10.1038/nn.3871